CHAPTER 5

Syntheses, Structures and Catecholase Activity of two Cobalt(III) Complexes Derived from *N*,*N*′-ethylenebis(3-ethoxysalicylaldiimine): A Special Host–Guest System from a Special Ligand

5.1. Introduction

Many mono/di/oligonuclear metal complexes have been reported from the following types of acyclic Schiff base ligands: (i) Single-compartmental ligands (H_2L^{Single}), obtained on [2+1] condensation of salicylaldehyde/2-hydroxyacetophenone/2-hydroxypropiophenone and a diamine;[1–11] (ii) Double-compartmental ligands H_2L^{OMe} [1,12–18]and H_2L^{OEt} [1,19–35] ligands, obtained on [2+1] condensation of 3-methoxysalicylaldehyde, and 3-ethoxysalicylaldehyde, respectively, and a diamine. It has been established that H_2L^{OEt} ligands are something special because its $O(phenoxo)_2O(ethoxy)_2$ compartment is strongly potential to act as a hydrogen bond acceptor with hydrogen bond donors such as water,[1,19–31] aquated proton,[32,33] ammonium ion,[22] and diprotonated diamine.[34,35] The metal complexes derived from H_2L^{OEt} ligands include mononuclear host–guest systems, dinuclear systems, double/triple/quadruple–decker compounds, supramolecular dimmers, and finite/infinite cocrystals.[1,19–35] It is worth mentioning that a number of the metal compounds derived from H_2L^{OEt} ligands are weak interaction directed self-assemblies[1,19–35] and thus lie in the domain of general perspectives of crystal engineering.[36–39] In spite of our extensive works on H_2L^{OEt} ligands[1,19–35] and in spite of our observation of a number of interesting self-assemblies over a decade, we have been hopeful that some more new types of weak interaction directed systems can be stabilized with this family of special ligands and therefore we are yet in the process of continuous development.

Although catechol oxidase, which catalyzes aerial oxidation of catechol to *o*-quinone, contains a dicopper(II) active site,[40,41] a number of functional model compounds of other metal ions are known to show this activity.[24,42–53] Those model compounds include manganese(II),[42] manganese(III),[24,43] manganese(IV),[44] manganese(III)manganese(II),[45] manganese(III)manganese(III),[46] iron(II),[47] iron(III),[48] cobalt(II),[49,50] cobalt(III)cobalt(II),[51–53] and cobalt(III)cobalt(III) systems.[53] In a recent report, a series of mononuclear manganese(III) compounds derived from H_2L^2 (*N*,*N*′-ethylenebis(3-ethoxysalicylaldiimine); (Chart 5.1) have been reported as functional models of catechol oxidase activity.[24] Role of auxiliary anionic ligands (azide, thiocyanate, chloride etc.) on the catechol oxidase activity has also been reported in that

investigation. We therefore have been interested to explore whether mononuclear cobalt(III) compounds derived from the same ligand show such activity.

With the above mentioned two-fold aims, namely, exploration of self-assembly aspects and catechol oxidase activity of mononuclear cobalt(III) complexes derived from H_2L^{OEt} ligand(s), we have isolated two Co^{III} compounds of composition $[Co^{III}L^2(N_3)_2 \supset (H_3O^+)]\cdot 2MeOH$ (**22**) and $[Co^{III}L^2(NCS)(H_2O)]\cdot DMF\cdot H_2O$ (**23**). Herein, we report syntheses, crystal structures and catechol oxidase activity of **22** and **23**, ESI-MS (positive) studies of **22** and uniqueness in the structure of **22**.

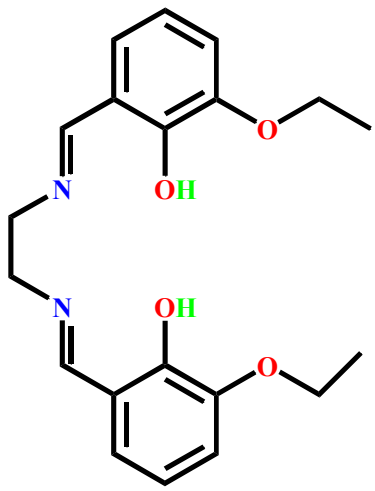

Chart 5.1. Chemical Structure of the Ligand $\mathbf{H_2L^2}$.

5.2. Experimental Section

5.2.1. Materials and Physical Measurements

All the reagents and solvents were purchased from the commercial sources and used as received. The Schiff base ligand H_2L^2 was prepared by 2:1 condensation of 3-ethoxysalicylaldehyde and ethylenediamine in MeOH.[20] Elemental (C, H and N) analyses were performed on a Perkin–Elmer 2400 II analyzer. IR spectra were recorded in the region 400–4000 cm^{-1} on Bruker-Optics Alpha-T spectrophotometer with samples as KBr disks. Studies on catecholase activity were performed with a Shimadzu UV-3600 spectrophotometer. The electrospray ionization mass spectra were recorded on a Micromass Qtof YA 263 mass spectrometer. Molar conductivity was measured at 25º C with a Systronics conductivity bridge. Magnetic susceptibility measurements of at 300 K were carried out with a Sherwood Scientific Co., U.K. magnetic susceptibility balance.

5.2.2. Syntheses

$[Co^{III}L^2(N_3)_2 \supset H_3O^+]\cdot 2MeOH$ (22). To a stirred solution of H_2L^2 (0.100 g, 0.28 mmol) in MeOH (15 mL), was dropwise added a MeOH solution of cobalt(II) perchlorate hexahydrate (0.205 g, 0.56 mmol). To the resulting brown solution, an aqueous solution (5 mL) of NaN_3 (0.074 g, 1.12 mmol) was added after 30 min. A dark brown precipitate started to deposit which was dissolved by heating. The solution was filtered to remove any suspended particles and the filtrate was kept at ambient temperature for slow evaporation. After 2─3 days, brown crystalline compound containing diffraction quality single crystals were deposited, which was collected by filtration and was washed with MeOH.

$[Co^{III}L^2(NCS)(H_2O)]\cdot DMF\cdot H_2O$ (23). To a stirred solution of H_2L^2 (0.100 g, 0.28 mmol) in MeOH (15 mL), was dropwise added a MeOH solution of cobalt(II) perchlorate hexahydrate (0.205 g, 0.560 mmol). To the resulting brown solution, an aqueous solution (5 mL) of NH_4SCN (0.085 g, 1.12 mmol) was added after 30 min. A dark brown precipitate started to deposit which was collected by filtration and washed with MeOH. Recrystallization was done on diffusing diethyl ether to DMF solution of the brown solid to yield crystalline compound containing diffraction quality single crystals.

5.2.3. Analytical and FT-IR Data

For **22**: Anal. Calcd for $C_{22}H_{33}N_8O_7Co$: C, 45.52; H, 5.73; N, 19.30%. Found: C, 45.38; H, 5.80; N, 19.45%. FT-IR on KBr (cm^{-1}): $\nu(H_3O^+)$, 3472 m and 3417 m; $\nu(N_3)$, 2018 vs; ν(C=N), 1635 s.

For **23**: Anal. Calcd for $C_{24}H_{33}N_4O_7SCo$: C, 49.65; H, 5.73; N, 9.65%. Found: C, 49.81; H, 5.67; N, 9.54%. FT-IR on KBr (cm^{-1}): $\nu(H_2O)$, 3446 m and 3267 m; ν(SCN), 2119 vs; ν(C=N), 1642 s.

5.2.4. Crystal Structure Determination

The crystallographic data for the two compounds, **22** and **23** are summarized in Table 5.1. Diffraction data of these two compounds were collected on a Bruker-APEX II CCD diffractometer at 296 K using graphite-monochromated Mo Kα radiation (λ = 0.71073 Å). For data processing and absorption correction the packages SAINT[54] and SADABS[54] were used. The structures were solved by direct and Fourier methods and refined by full-matrix least-squares based on F^2 using SHELXTL[55] and SHELXL-97 packages.[56] The three hydrogen atoms of the oxonium ion in **22** and the two hydrogen atoms of the coordinated water molecule in **23** were located from Fourier difference maps. The following hydrogen atoms could not be located: One hydroxyl hydrogen atom (linked with O5) of one of the two methanol molecules in **22**; Two hydrogen atoms linked with the solvated water oxygen atom (O7) in **23**. All other hydrogen atoms in the

two compounds were inserted on geometrical calculated positions with fixed thermal parameters and were refined isotropically, while all the nonhydrogen atoms were refined anisotropically. The final least-squares refinements (R_1) based on $I > 2\sigma(I)$ converged to 0.0563 and 0.0576 for **22** and **23**, respectively.

Table 5.1. Crystallographic Data for $[Co^{III}L^2(N_3)_2 \supset H_3O^+] \cdot 2MeOH$ (**22**) and $[Co^{III}L^2(NCS)(H_2O)] \cdot DMF \cdot H_2O$ (**23**).

	22	**23**
empirical formula	$C_{22}H_{32}N_8O_7Co$	$C_{24}H_{31}N_4O_7SCo$
fw	579.49	578.52
crystal system	orthorhombic	triclinic
space group	*Pbca*	$P\bar{1}$
a (Å)	16.823(2)	10.889(4)
b (Å)	11.1895(16)	11.834(4)
C (Å)	28.186(4)	28.186(4)
α (deg)	90.00	116.917(4)
β (deg)	90.00	92.120(4)
γ (deg)	90.00	105.574(4)
V (Å^3)	5305.7(13)	1342.8(8)
Z	8	2
ρ_{calcd} (g cm^{-3})	1.451	1.431
μ (mm^{-1})	0.704	0.766
T (K)	296(2)	296(2)
F (000)	2424	604
2θ (deg)	2.88–49.94	3.76–50.00
Index ranges	$-19 \le h \le 19$	$-12 \le h \le 12$
	$-12 \le k \le 13$	$-14 \le k \le 14$
	$-33 \le l \le 33$	$-13 \le l \le 14$
Reflections collected	34702	9194
Independent reflections(R_{int})	4641(0.0379)	4605(0.0388)
Parameters refined	363	346
Goodness-of-fit on F^2	1.054	1.061
$R_1{}^a$, w$R_2{}^b$ ($I > 2\sigma(I)$)	0.0563, 0.2008	0.0576,0.1619
$R_1{}^a$, w$R_2{}^b$ (for all data)	0.0714, 0.2261	0.0773,0.1834

$^a R_1 = [\sum||F_o| - |F_c||/\sum|F_o|]$. $^b wR_2 = [\sum w(F_o^2 - F_c^2)^2/\sum wF_o^4]^{1/2}$.

5.3. Results and Discussion

5.3.1. Syntheses and Characterization

The two mononuclear cobalt(III) complexes **22** and **23** were prepared by the reaction of the ligand (H_2L^2) with $Co(ClO_4)_2{\cdot}6H_2O$ and NaN_3 (for **22**)/ and NH_4SCN (for **23**) in 1:2:4 ratio. Clearly, aerial oxidation of cobalt(II) to cobalt(III) and metal assisted deprotonation of the phenolic moieties take place during the formation of **22** and **23**. It is worth mentioning that two Co^{III} compounds derived from H_2L^{OEt} ligands have been reported previously.[57,58] Those are produced on reacting the corresponding ligand with $CoCl_2{\cdot}6H_2O$[58] or $Co(ClO_4)_2{\cdot}6H_2O$.[57] In both those cases a fraction of H_2L^{OEt} ligand decomposes to give rise to either the aldehyde or the half–condensed ligand (aldehyde:diamine = 1:1). In contrast, no such ligand decomposition takes place in case of **22** or **23**, probably because azide and thiocyanate are used as auxiliary ligand in the syntheses of these two compounds. The characteristic C=N stretching frequency is observed as a strong band at 1635 cm^{-1} for the complex **22** and 1642 cm^{-1} **23**. The presence of azide in **22** and thiocyanate in **23** is evidenced by the appearance of a band of very strong intensity at 2018 and 2119 cm^{-1}, respectively. O–H stretching of water and oxonium ion in **23** and **22**, respectively, is observed as a broad band at 3446 and 3472 cm^{-1} with a shoulder at 3267 and 3417 cm^{-1}. Compound **23** is practically insoluble in common organic solvents except DMF, while compound **22** is soluble in DMF and MeCN. Therefore, all the solution studies of **22** were carried out in DMF and MeCN, while for **23**, the solution studies were performed in DMF only. The molar conductivity values of the two compounds **22** and **23** are 9.3 and 18.9 $\Omega^{-1}M^{-1}cm^{-1}L$ respectively in DMF and 6.3 $\Omega^{-1}M^{-1}cm^{-1}L$ for compound **22** in MeCN. The molar conductivity values indicates that compound **22** in DMF and MeCN and compound **23** in DMF retains their non-electrolyte behavior.[59] The UV-Vis spectra of 0.125×10^{-4} M and 2×10^{-3} M solutions of complexes **22** (in DMF and MeCN), and **23** (in DMF) were measured and the band position and extinction coefficient are listed in Table 5.2. For complex **22**, there are three bands in the range 248–355 nm (ε = 12800–54160 $M^{-1}cm^{-1}$) in MeCN but only two bands in the range 264–352 nm (ε = 12800–38400 $M^{-1}cm^{-1}$) in DMF. For complex **23** in DMF, three bands are observed in the range 264–404 nm (ε = 8000–46000 $M^{-1}cm^{-1}$). All

these bands arise due to internal ligand transition or ligand to metal charge transfer. The two compounds exhibit one low intensity band at 621 nm which is clearly due to the d-d band of Co^{III} center. Room temperature magnetic moment was measured for the two complexes; the value of μ_{eff} implies that both are diamagnetic in nature.

Table 5.2. Band position (λ_{max} (nm)) and Extinction Coefficient Values (ε $M^{-1}cm^{-1}$) of UV-Vis Bands of the compounds **22** and **23** in DMF and MeCN.

	d-d bands				**Internal ligand/ ligand to metal transitions**											
	In DMF		**In MeCN**		**In DMF**						**In MeCN**					
	λ_{max}	ε	λ_{max}	ε	λ_{max}	ε	λ_{max}	ε	λ_{max}	ε	λ_{max}	ε	λ_{max}	ε	λ_{max}	ε
22	621	370	621	265	352	12800	264	38400	—	—	355	14000	283	12800	248	54160
23	621	302	—	—	404	8000	345	10400	264	46000	—	—	—	—	—	—

5.3.2. Description of Crystal Structures of 22 and 23

Crystal structures of $[Co^{III}L^2(N_3)_2\supset(H_3O^+)]\cdot 2MeOH$ (**22**) and $[Co^{III}L^2(NCS)(H_2O)]\cdot DMF\cdot H_2O$ (**23**) are shown in Figures 5.1 and 5.2, respectively. The structures reveal that both **22** and **23** are mononuclear cobalt(III) compounds containing $[L^2]^{2-}$. The metal center in both the compounds occupies the $N(imine)_2O(phenoxo)_2$ compartment of $[L^2]^{2-}$.

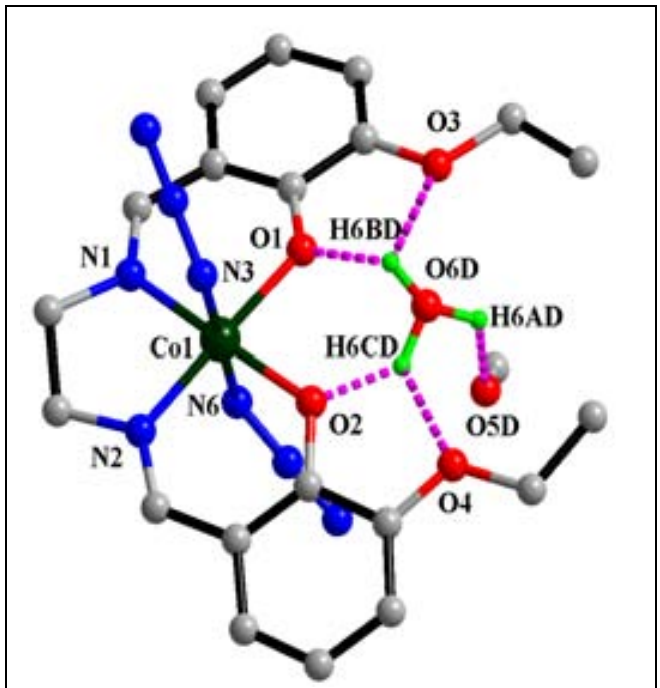

Figure 5.1. Crystal structure of $[Co^{III}L^2(N_3)_2\supset H_3O^+]\cdot 2MeOH$ (**22**). All the hydrogen atoms, except those participate in hydrogen bonding, are omitted for clarity. Symmetry: D, –1+x, y, z.

Figure 5.2. Crystal structure of $[Co^{III}L^2(NCS)(H_2O)]\cdot DMF\cdot H_2O$ (**23**). All the hydrogen atoms except those of coordinated water molecule, and the solvated DMF and water molecules are omitted for clarity.

In both the compounds, cobalt(III) center is hexacoordinated; the additional two coordination sites are satisfied by two nitrogen atoms of two terminal azide ligands in **22**, while those are satisfied by the nitrogen atom of a terminal thiocyanate ligand and the oxygen atom of a water molecule in **23**. While $[Co^{III}L^2(NCS)(H_2O)]$ (**23**; excluding solvent molecules) is a neutral system, charge of $[Co^{III}L^2(N_3)_2]$ moiety (a part of **22**) is −1 and this negative charge is balanced by an oxonium ion (H_3O^+) in compound **22**. The oxonium ion in this compound is trapped in the $O(phenoxo)_2O(ethoxy)_2$ compartment by forming hydrogen bonds; each of the two of the three hydrogen atoms in H_3O^+ forms bifurcated hydrogen bonds with a phenoxo and an ethoxy oxygen atoms. Compound **22** contains two methanol molecules as solvent of crystallization, one of which is interlinked with the trapped oxonium ion by hydrogen bonding interactions; the third hydrogen atom of the oxonium ion forms a hydrogen bond with the oxygen atom of one methanol

molecule. In **23**, coordinated water molecule interacts with the $O(phenoxo)_2O(ethoxy)_2$ compartment of a neighboring symmetry related complex by forming hydrogen bonds (Figure 5.3); each of the two water hydrogen atoms forms bifurcated hydrogen bonds with one phenoxo and one ethoxy oxygen atoms. There are also two π····π stacking interactions in **23** between the two neighboring aromatic rings, where the center-to-center distance and dihedral angle between the least-squares planes of the adjacent aromatic rings are 3.630 Å and 5.01º respectively. This way, two symmetry related mononuclear cobalt(III) complex units are interlinked to form dimer-of-mononuclear type self-assembly in **23**.

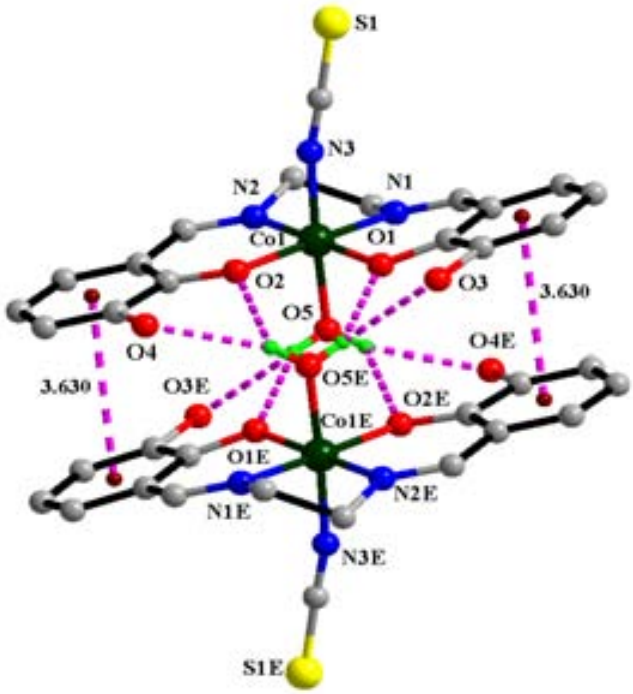

Figure 5.3. Perspective view of the dimeric self-assembly of **23**. Ethoxy carbon atoms, the solvated DMF and water molecules and the hydrogen atoms, except those participating in hydrogen bonding, are omitted for clarity. Symmetry: E, 1–x, – y, 1–z. Bond lengths are shown in Å.

Selected bond lengths and bond angles in the coordination environment of the metal center in **22** and **23** are listed in Table 5.3 in a comparative way, while the individual bond lengths and bond angles of the metal centers are listed in Tables 5.4 and 5.5 for compound **22** and **23**, respectively. The coordination geometry of the metal center in both the compounds is distorted octahedral in which the $N(imine)_2O(phenoxo)_2$ compartment defines the basal plane. Two Co^{III}–O(phenoxo) and two Co^{III}–N(imine) bond distances in compound **22** as well as in compound **23** are very close. Again, the Co^{III}–O(phenoxo) / N(imine) bond distances in both the compounds are also very close. The overall range of these bond distances in the two compounds is 1.875−1.902 Å. The Co^{III}–N(NCS) bond distance, 1.887 Å, in **23** is almost same as those in the basal plane, while the other apical bond distance (Co^{III}–O(water) = 1.934 Å) in this compound is slightly longer. In the case of **22**, both the apical Co^{III}–N(azide) bond distances (1.962 and 1.983 Å) are clearly longer than those in the basal plane. For both the compounds, both the *cisoid* (84.36−95.02° in **22**; 85.08−94.15° in **23**) and *transoid* angles (178.32−179.41° in **22**; 176.85−178.42° in **23**) don't deviate much from the ideal values. The average deviation ($d_{N/O}$ = 0.018 Å in **22**; 0.008 Å in **23**) of the imine nitrogen and phenoxo oxygen atoms and displacement (d_{Co}= 0.008 Å in **22**; 0.028 Å in **23**) of the metal center from the least-squares $N(imine)_2O(phenoxo)_2$ basal plane is very small. All in all, it is evident that the coordination geometry of the cobalt(III) center in both **22** and **23** is deviated only little from the ideal octahedral geometry. Two phenoxo and two ethoxy oxygen atoms in both the compounds form almost a perfect plane, as evidenced by the small values (0.035 Å for **22** and 0.105 Å for **23**) of the average deviation of the constituting oxygen atoms from the least-squares $O(phenoxo)_2O(ethoxy)_2$ plane. The oxygen atom of the oxonium ion in **22** is displaced by 0.277 Å from the least-squares $O(phenoxo)_2O(ethoxy)_2$ plane.

Table 5.3. Comparative Structural Parameters (Distances in Å and Angles in deg) in the Coordination Environment of the Co^{III} Center in **22** and **23**.

Parameters	**22**	**23**
Co–O(phenoxo)	1.897(3), 1.883(3)	1.895(3), 1.902(3)
Co–N(imine)	1.875(3), 1.882(3)	1.885(3), 1.885(3)
Co–First axial	Co–N(N_3) = 1.983(4)	Co–O(water) = 1.934(3)
Co–Second axial	Co–N(N_3) = 1.962(4)	Co–N(NCS) = 1.887(4)
All *trans* angles' range	178.32(15)–179.41(16)	176.85(12)–178.42(12)
All *cis* angles' range	84.36(11)–95.02(13)	85.08(14)–94.15(13)
d_{Co} [a]	0.008	0.028
$d_{N/O}$ [a]	0.018	0.008
d_{O} [a]	0.035	0.105

[a] d_{Co}, $d_{N/O}$ and d_{O} are the displacement of the metal center, the average deviation of the constituent atoms from the corresponding least-squares basal $N(imine)_2O(phenoxo)_2$ plane and the average deviation of the constituent atoms from the corresponding least-squares O_4 plane repectively.

Table 5.4. Selected Bond Lengths (Å) and Angles (deg) of $[Co^{III}L^{2}(N_3)_2 \supset H_3O^{+}]\cdot 2MeOH$ (**22**).

Co1–O1	1.897(3)
Co1–O2	1.883(3)
Co1–N1	1.875(3)
Co1–N2	1.882(3)
Co1–N3	1.983(4)
Co1–N6	1.962(4)
O1–Co1–N2	178.32(15)
O2–Co1–N1	178.86(13)
N3–Co1–N6	179.41(16)
O1–Co1–N1	94.67(13)
N2–Co1–N1	85.97(14)
N2–Co1–O2	95.02(13)
O1–Co1–O2	84.36(11)
O1–Co1–N3	90.28(14)
O2–Co1–N3	88.17(14)
N1–Co1–N3	91.25(15)
N2–Co1–N3	91.26(15)
O1–Co1–N6	89.69(15)
O2–Co1–N6	92.41(14)
N1–Co1–N6	88.17(16)
N2–Co1–N6	88.77(15)

Table 5.5. Selected Bond Lengths (Å) and angles (deg) of $[Co^{III}L^2(NCS)(H_2O)]\cdot DMF\cdot H_2O$ (**23**).

Co1–O1	1.895(3)
Co1–O2	1.902(3)
Co1–N1	1.885(3)
Co1–N2	1.885(3)
Co1–N3	1.887(4)
Co1–O5	1.934(3)
O1–Co1–N2	178.42(12)
O2–Co1–N1	177.67(12)
N3–Co1–O5	176.85(12)
O1–Co1–N1	93.86(13)
N2–Co1–N1	85.08(14)
N2–Co1–O2	94.15(13)
O1–Co1–O2	86.86(11)
O1–Co1–N3	90.16(13)
O2–Co1–N3	92.80(13)
N1–Co1–N3	89.42(14)
N2–Co1–N3	91.01(15)
O1–Co1–O5	89.61(12)
O2–Co1–O5	90.32(12)
N1–Co1–O5	87.47(13)
N2–Co1–O5	89.17(14)

The parameter values of the hydrogen bonds in **22** and **23** are listed in Table 5.6. Although the D····A contacts for the oxonium ion····O(phenoxo/ethoxy) hydrogen bonds in **22** lie in the range 2.320−2.607 Å, the D–H····A angles are smaller, 83.86−132.50°, indicating that these hydrogen bonds are moderately strong. The oxonium ion····methanol hydrogen bond (D····A= 2.419 Å, D–H····A= 120.04°) are also moderately strong. In the case of **23**, the water····O_4 hydrogen bonds are also moderately strong; the ranges of D····A contacts and D–H····A angles are 2.720−3.041 Å and 130.49−151.54°.

Table 5.6. Geometries (Distances in Å and Angles in deg) of Hydrogen Bonds in **22** and **23**. Symmetry: D, –1+x, y, z; E, 1– x, – y, 1 – z.

	D–H···A	**D···A**	**H···A**	**D–H···A**
22	O6D–H6BD···O3	2.607	2.538	83.86
	O6D–H6BD···O1	2.320	1.892	105.76
	O6D–H6CD···O2	2.332	1.591	132.50
	O6D–H6CD···O4	2.600	2.016	118.50
	O6D–H6CD···O5D	2.419	1.816	120.04
23	O5–H5WA···O4E	3.026	2.302	151.54
	O5–H5WA···O2E	2.821	2.184	137.20
	O5–H5WB···O3E	3.041	2.468	130.49
	O5–H5WB···O1E	2.720	2.009	149.52

Bond valence sum (BVS) calculations of the Co^{III} center of **22** and **23** have been performed. The values are 3.93 and 4.4 for **22** and **23**, respectively. The values are much larger than 3 but such large BVS values of Co^{III} centers are not unusual.[51,53,60]

As already mentioned, a number of mononuclear M^{III} compounds are known from H_2L^{OEt} ligands.[1,19,24–26,57,58,61–70] The trivalent metal ion, which resides in $N(imine)_2O(phenoxo)_2$ compartment, in all of those compounds is either Fe^{III} or Mn^{III} [24–26,61–70] and it is Co^{III} in only two cases.[57,58] In those two examples of the cobalt(III) compounds, ligand decomposition takes place and the fifth and sixth coordination positions are occupied by phenolate oxygen atom and aldehyde oxygen atom or imine nitrogen atom of the decomposed ligand. In the case of one of the several manganese(III) compounds, the fifth and sixth coordination positions are occupied by a chelating anionic ligand, acetate.[66] In all other cases, the general composition of the M^{III} (clearly, Mn^{III}/Fe^{III}) compounds are either $[M^{III}L^{OEt}(H_2O)(S)]Y$ or $[M^{III}L^{OEt}(H_2O)(X)]$ where S is water,[26,64,65,69] or methanol,[25,26] Y is an anion such as nitrate[26,64,65] or perchlorate [25,26,69] and X is an anionic ligand such as acetate,[24,61,64,70] azide,[24,25,68] chloride,[24,25,63,67] thiocyanate [24,62] and selenocyanate.[24] A common feature in these latter two types of compounds is that at least one water molecule is coordinated with the M^{III} center (which occupies N_2O_2 compartment) and that water molecule interacts with the O_4 compartment

of the neighboring symmetry related molecule to form dimer-of-mononuclear type structure.[24–26,61–65,67–70]

It is well known now that $O(phenoxo)_2O(ethoxy)_2$ compartment in copper(II)/nickel(II) systems derived from H_2L^{OEt} ligands can accommodate a noncoordinated guest species such as water, aquated proton, ammonium ion and diprotonated diamine.[1,19–35] In contrast, it is quite unlikely that a noncoordinated guest species (water, oxonium ion, etc.) be incorporated in the O_4 compartment of mononuclear M^{III} compounds of H_2L^{OEt} ligands. If otherwise, that would be definitely an unexpected and interesting observation. Of the two Co^{III} compounds in this investigation, the composition of $[Co^{III}L^2(NCS)(H_2O)]\cdot DMF\cdot H_2O$ (**23**) belongs to the expected general composition $[M^{III}L^{OEt}(H_2O)(X)]$ and its coordinated water molecule interacts as usual with the O_4 compartment of neighboring symmetry related molecule (Figure 5.3). However, $[Co^{III}L^2(N_3)_2\supset(H_3O^+)]\cdot 2MeOH$ (**22**) represents a new type of composition. Unlike in all the previous M^{III} compounds, both the two axial ligands in **22** are anionic (azide). Therefore, an oxonium ion is present in this molecule to balance charges. Existence of oxonium ion as charge balancing cation is very usual in various compounds.[1] But, as the $O(phenoxo)_2O(ethoxy)_2$ compartment is strongly potential to form hydrogen bonds, the oxonium ion in **22** is trapped in the O_4 compartment. As a matter of fact, compound **22** is the first example of a M^{III} compound of H_2L^{OEt} ligands where a noncoordinated guest species (oxonium ion here) is trapped in the $O(phenoxo)_2O(ethoxy)_2$ compartment. Another unique aspect is the presence of two apical anionic ligands. Several mononuclear M^{III} compounds (M= Mn^{III}, Fe^{III}, Co^{III}) having the metal ion in the $N(imine)_2O(phenoxo)_2$ compartment are known derived from double-compartmental acyclic Schiff base ligands (both 3-ethoxysalicylaldehyde─diamine and 3-methoxysalicylaldehyde─diamine).[1,24–26,57,58,61–70] In none of those compounds, the M^{III} center is coordinated with two apical anionic ligands as in **22**. Clearly, **22** represent a new type from that aspect also.

5.3.3. Catecholase Activity

In most of the catecholase activity studies, 3,5-di-*tert*-butylcatechol (3,5-$DTBCH_2$) has been employed as the model substrate because (i) It is easily oxidized to 3,5-DTBQ and (ii) the generated product, 3,5-di-*tert*-butylquinone (3,5-DTBQ), has a characteristic absorption band at around 400 nm.[24,40–53] Therefore, activity and kinetic parameters can be determined by monitoring the absorption maximum of the quinone.

Catecholase activity studies were performed in both DMF and MeCN for compound **22** and only in DMF for compound **23**. A solution (0.25×10^{-4} M) of a complex in MeCN/DMF was treated with a 100-fold concentrated solution (in the same solvent) of 3,5-$DTBCH_2$ and the course of the reaction was followed by recording UV-Vis spectra of the mixture under aerobic condition. The spectra of the mixture of a complex and 3,5-$DTBCH_2$ were recorded after every 5 min up to a total time of 90 min. As already mentioned (Table 5.2), complex **22** has an intense band at 355 nm (in MeCN) which is gradually red shifted to 400 nm with steady increase in intensity after mixing with 3,5-$DTBCH_2$, indicating more and more formation of 3,5-DTBQ (Figure 5.4). It has also been mentioned that complex **23** (in DMF) shows two intense signals at 404 and 345 nm (Table 5.2). After mixing with 3,5-$DTBCH_2$, both these two peaks become blue/red shifted initially and then merged at 400 nm (Figure 5.5). However, steady increase in intensity of the two bands or the single merged band takes place after mixing with 3,5-$DTBCH_2$. The observation here also in line with more and more formation of 3,5-DTBQ because, as already mentioned, it is well known that 3,5-DTBQ shows an intense band at around 400 nm.[24,40–53] Clearly, complex **22** in MeCN and complex **23** in DMF show catechol oxidase activity. At this point, it is relevant to mention that blank experiment without complex showed no formation of the quinone up to 12 h in MeCN and 3 h in DMF. After mixing complex **22** with 3,5-$DTBCH_2$ in DMF, no band around 400 nm is generated, indicating that complex **22** in DMF does not show catechol oxidase activity.

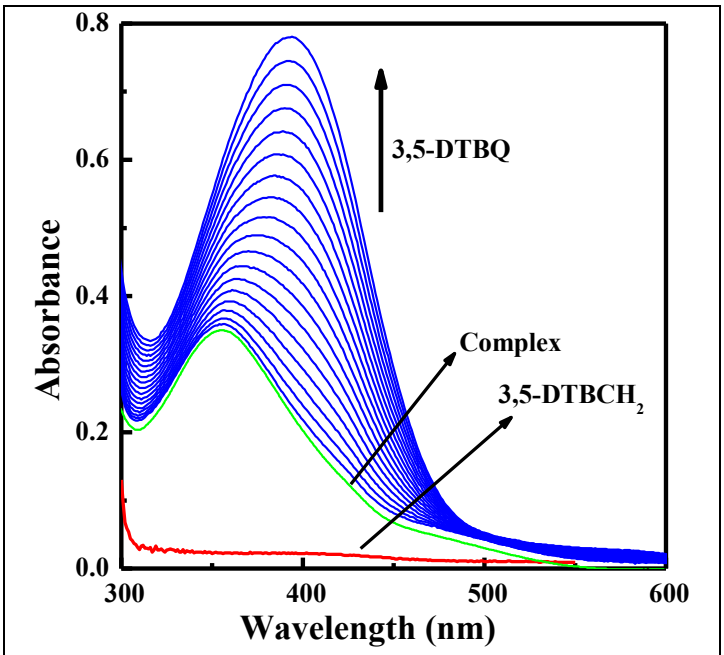

Figure 5.4. Spectral profile showing the increase of quinone band at 400 nm after the addition of 100 fold of 3,5-DTBCH$_2$ to a solution containing complex **22** (0.25×10^{-4} M) in MeCN. Spectra were recorded after each 5 min.

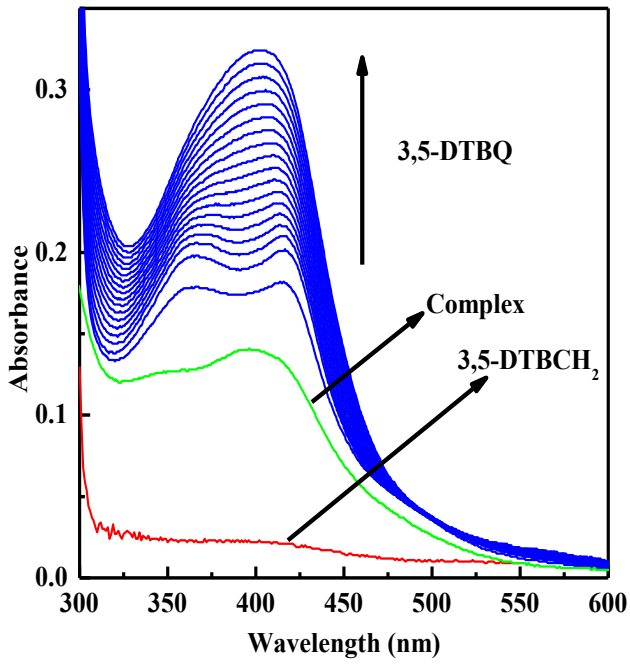

Figure 5.5. Spectral profile showing the increase of quinone band at 400 nm after the addition of 100 fold of 3,5-DTBCH$_2$ to a solution containing complex **23** (0.25×10^{-4} M) in DMF. Spectra were recorded after each 5 min.

Kinetic studies of the catecholase activity of the catalysts, complexes **22** (in MeCN) and **23** (in DMF), have been performed to understand the extent of their efficiency. For this purpose, 0.25×10^{-4} M solution of a complex in respective solvent was treated with the 3,5-DTBCH$_2$ solution of concentration ranging from 0.25×10^{-3} M to 0.25×10^{-2} M. For a particular complex–substrate mixture, time scan at the maximum of the quinone band was carried out for a period of 90 min at a constant temperature, 25 ºC. The optical density of 3,5-DTBQ is associated with that of the original band of the complex species, so optical density obtained in the time scan was subtracted by the optical density of the original complex at the wavelength at which time scan was monitored. This difference in optical densities was plotted against time and the rate constant for a catalyst complex was determined from that plot by initial rate method. The rate constant versus substrate concentration data were then analyzed on the basis of the Michaelis–Menten approach of enzymatic kinetics to get the Lineweaver–Burk plot as well as the values of the parameters V_{max}, K_M, and K_{cat}. Observed and simulated initial

rate versus [substrate] plots and the Lineweaver–Burk plots for the complexes **22** (in MeCN) and **23** (in DMF) are shown in Figures 5.6 and 5.7, respectively. As listed in Table 5.7, turnover numbers (K_{cat}) are 10.0 h^{-1} for complex **22** in MeCN and 11.2 h^{-1} for complex **23** in DMF. Clearly, complex **22** in MeCN and complex **23** in DMF are functional models of catechol oxidase.

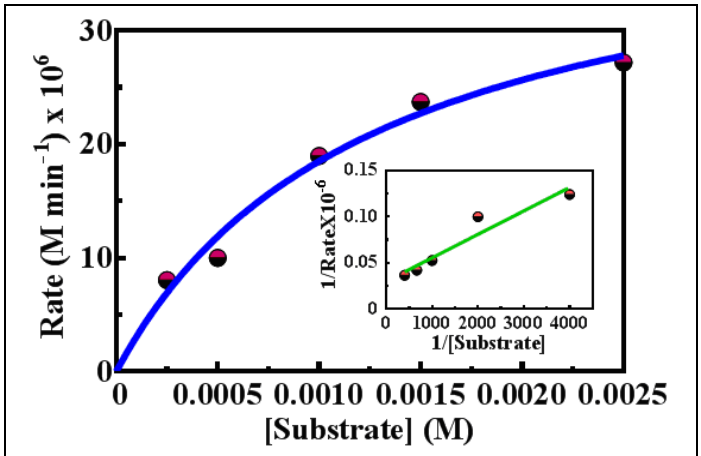

Figure 5.6. Initial rates versus substrate concentration for the 3,5-DTBCH$_2$ → 3,5-DTBQ oxidation reaction catalyzed by complex **22** in MeCN. Inset shows Lineweaver-Burk plot. Symbols and solid lines represent the observed and simulated profiles, respectively.

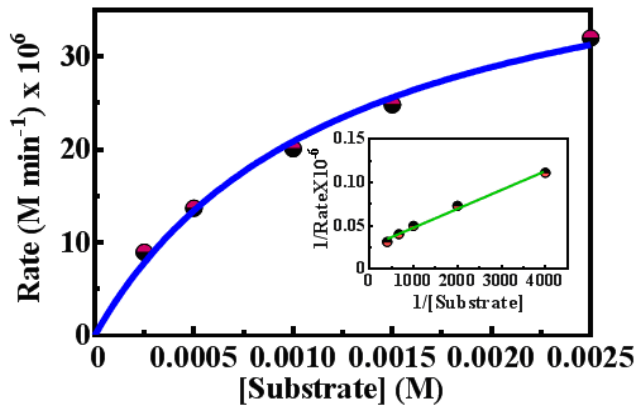

Figure 5.7. Initial rates versus substrate concentration for the 3,5-DTBCH$_2$ → 3,5-DTBQ oxidation reaction catalyzed by complex **23** in DMF. Inset shows Lineweaver-Burk plot. Symbols and solid lines represent the observed and simulated profiles, respectively.

Table 5.7. Kinetic Parameters for the Complexes **22** and **23**.

	Solvent	V_{max} **(M min^{-1})**	**Std.Error**	K_M **(M)**	**Std.Error**	K_{cat} **(h^{-1})**
22	MeCN	4.18×10^{-6}	5.15×10^{-7}	1.26×10^{-3}	3.28×10^{-4}	10.0
23	DMF	4.68×10^{-6}	3.55×10^{-7}	1.24×10^{-3}	2.08×10^{-4}	11.2

5.3.4. Electrospray Ionization Mass Spectral Study

The electrospray ionization mass spectrum in positive mode (ESI-MS positive) of MeCN solution of **22** was recorded. ESI-MS of complex **23** could not be recorded as it is not soluble in low boiling solvents. The observed and simulated spectra of complex **22** are shown in Figure 5.8 and the assigned species are listed in Table 4.8. Compound **22** exhibits five peaks at *m*/*z* = 413 (100%, line to line separation 1.0), 436 (70%, line to line separation 1.0), 826 (30%, line to line separation 1.0), 843 (15%, line to line separation 1.0) and 868 (35%, line to line separation 1.0). These five peaks can be assigned as follows: (i) *m*/*z* = 413, a mononuclear Co^{III} species $[Co^{III}L^2]^+$ (**I**; $C_{20}H_{22}N_2O_4Co$); (ii) *m*/*z* = 436, a $Co^{II}Na^{I}$ species $\{[Co^{II}L^2]+Na^+\}$ (**II**; $C_{20}H_{22}N_2O_4CoNa$); (iii) *m*/*z* = 826, a composition containing both a Co^{III} and Co^{II} moieties $\{[Co^{III}L^2]+[Co^{II}L^2]\}^+$ (**III**; $C_{40}H_{44}N_4O_8Co_2$) – probably an aggregate between the two; (iv) *m*/*z* = 843, a hydroxo bridged dinuclear Co^{III} species $[(Co^{III}L^2)_2(OH)]^+$ (**IV**; $C_{40}H_{45}N_4O_9Co_2$); (v) *m*/*z* =868, an azide-bridged dinuclear Co^{III} species $[(Co^{III}L^2)_2(N_3)]^+$ (**V**; $C_{40}H_{44}N_7O_8Co_2$).

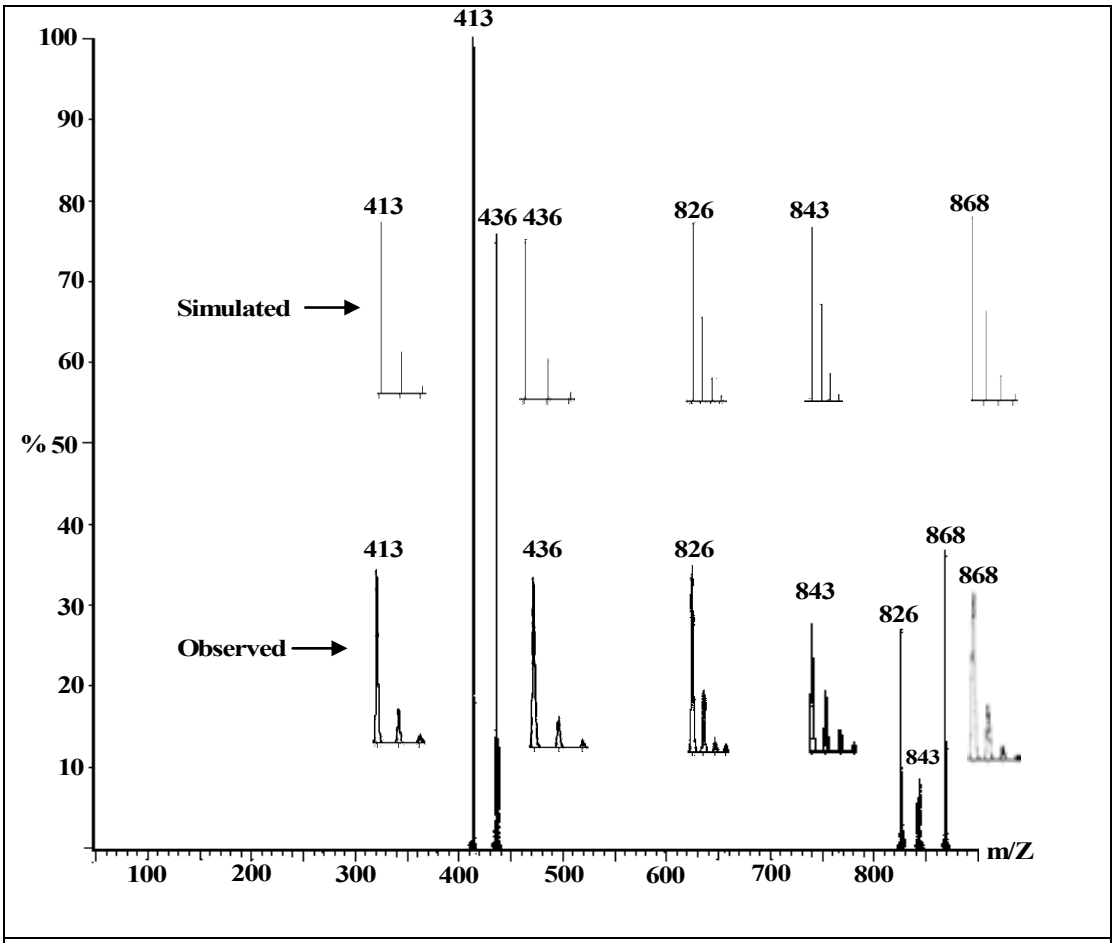

Figure 5.8. Electrospray ionization mass spectrum (ESI-MS positive) of $[Co^{III}L^{2}(N_3)_2 \supset H_3O^{+}]\cdot 2MeOH$ (**22**) in MeCN showing observed and simulated isotopic distribution patterns.

Table 5.8. The Composition, Empirical Formula, Peak Position and Relative Peak Intensity of the Species in the ESI-MS Positive Spectra of **22** in MeCN.

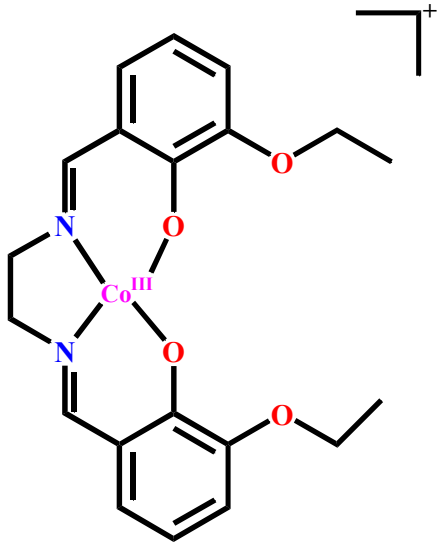	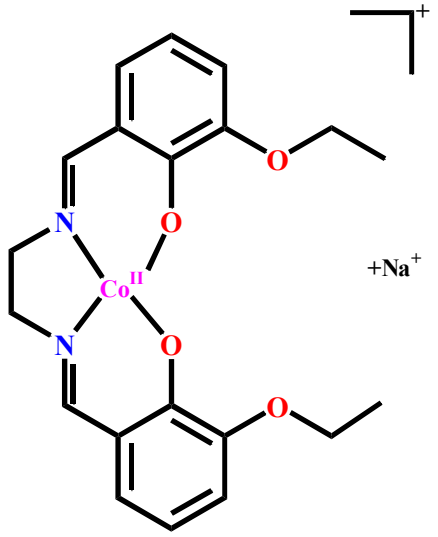
$[Co^{III}L^{2}]^{+}$ (**I**; $C_{20}H_{22}N_2O_4Co$) m/z = 413, Intensity = 100%	$\{[Co^{II}L^{2}]+Na^{+}\}$ (**II**; $C_{20}H_{22}N_2O_4CoNa$) m/z =436, Intensity = 70%
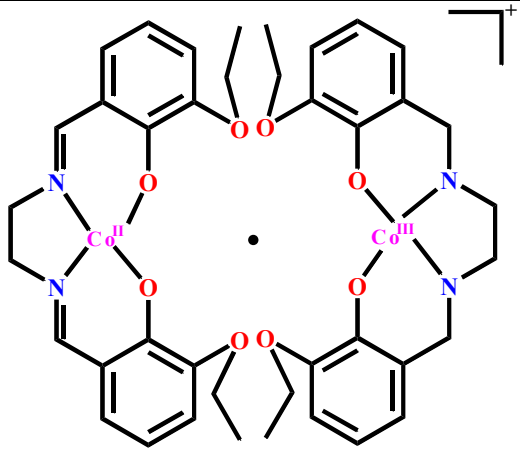	
$\{[Co^{III}L^{2}]+[Co^{II}L^{2}]\}^{+}$ (**III**; $C_{40}H_{44}N_4O_8Co_2$) m/z = 826, Intensity = 30%	

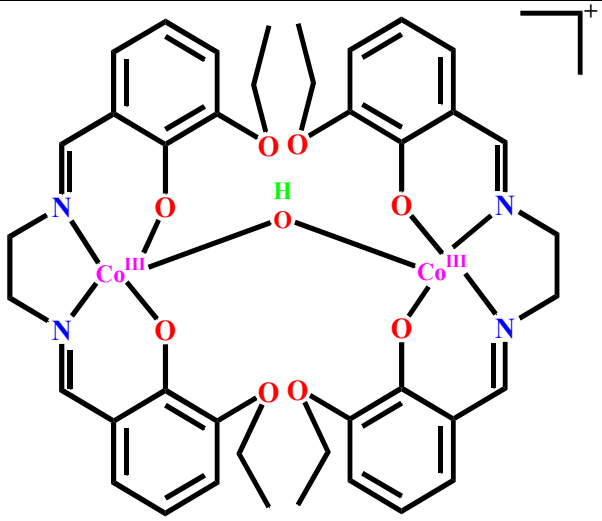

$[(Co^{III}L^2)_2(OH)]^+$
(**IV**; $C_{40}H_{45}N_4O_9Co_2$)
m/z = 843, Intensity = 15%

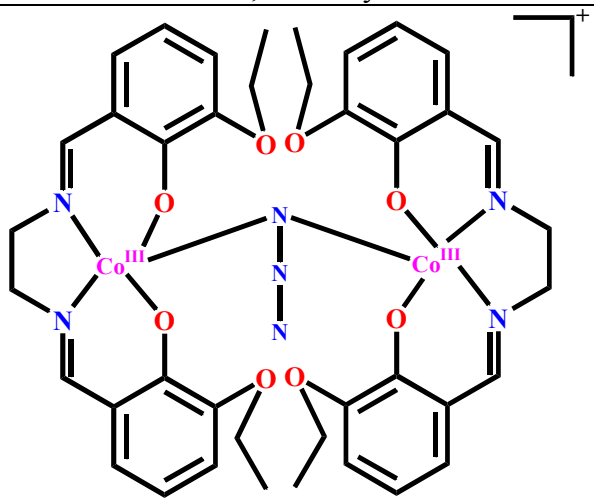

$[(Co^{III}L^2)_2(N_3)]^+$
(**V**; $C_{40}H_{44}N_7O_8Co_2$)
m/z = 868, Intensity = 35%

Coordination of catechol moiety to the metal center during the catalytic cycle by any possible way is an essential criterion to show catecholase activity. It is worth mentioning that the intermediate species identified from ESI-MS spectra (or in solid state) may not be a real intermediate during the catalytic cycle in solution. However, ESI-MS can give an idea about the possible intermediates in catalytic cycle. Therefore, we have recorded the ESI-MS spectrum of a mixture of **22** and 3,5-$DTBCH_2$ in MeCN after 15 min of mixing to check if any complex─substrate aggregate could be identified. The observed and simulated spectra of the mixture of compound **22** and a 100-fold 3,5-$DTBCH_2$ are shown in Figure 5.9 and the assigned species are listed in Table 5.9. The mixture exhibits five peaks, at m/z = 243 (100%, line to line separation 1.0), 413 (20%, line to line separation 1.0), 436 (28%, line to line separation 1.0), 463 (75%, line to line separation 1.0) and 853 (5%, line to line separation 1.0). Among these five peaks, the peaks at m/z = 413 and m/z = 436 are also observed in the spectrum of the original complex. Three other peaks can be assigned as follows: (i) m/z = 243, a 1:1 quinone─sodium aggregate $[(3,5\text{-DTBQ})Na]^+$ (**VI**; $C_{14}H_{20}O_2Na$); (ii) m/z = 463, a 2:1 quinone─sodium aggregate $[(3,5\text{-DTBQ})_2Na]^+$ (**VII**; $C_{28}H_{40}O_4Na$); (iii) m/z = 853, a mononuclear Co^{II} species $[Co^{II}L^2(3,5\text{-DTBQ})_2+H^+]^+$ (**VIII**; $C_{48}H_{63}N_2O_8Co$). It is worth mentioning that the identification of the two quinone species (**VI** and **VII**) as well as a Co^{III}–quinone aggregate (**VIII**) in the ESI-MS spectra of complex **22** is in line with the catecholase activity of the complex.

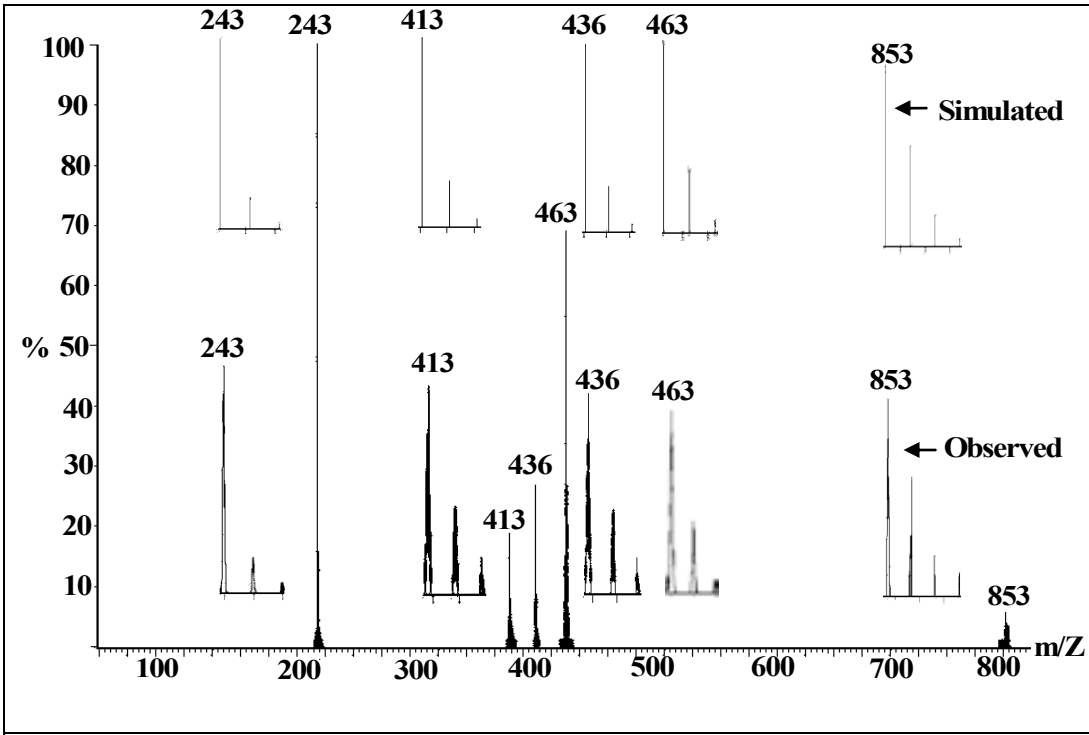

Figure 5.9. Electrospray ionization mass spectrum (ESI-MS positive) of a 1:100 mixture of $[Co^{III}L^{2}(N_3)_2 \supset H_3O^+]\cdot 2MeOH$ (**22**) and 3,5-DTBCH$_2$ in MeCN recorded after 15 min of mixing, showing observed and simulated isotopic distribution patterns.

Table 5.9. The Composition, Empirical Formula, Peak Position and Relative Peak Intensity of the Species in the ESI-MS Positive Spectra of **22** and 3,5-DTBCH$_2$ in MeCN.

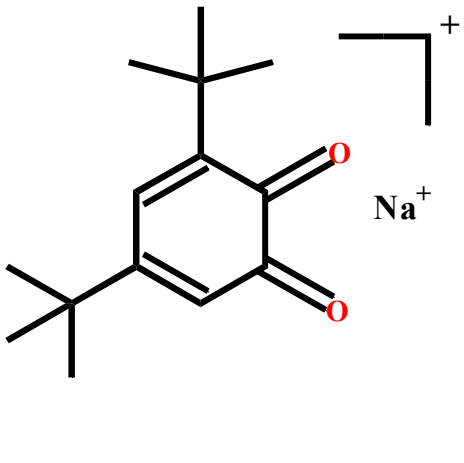	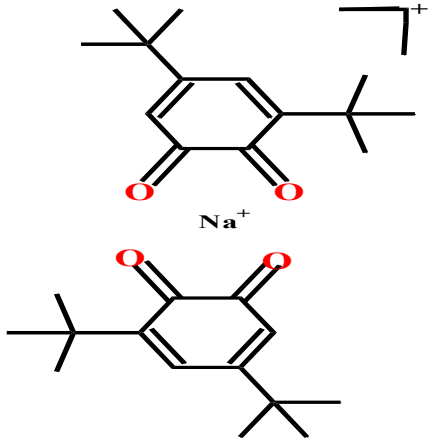
$[(3,5\text{-DTBQ})Na]^+$ (**VI**; $C_{14}H_{20}O_2Na$) m/z = 243, Intensity = 97%	$[(3,5\text{-DTBQ})_2Na]^+$ (**VII**; $C_{28}H_{40}O_4Na$) m/z = 463, Intensity = 75%

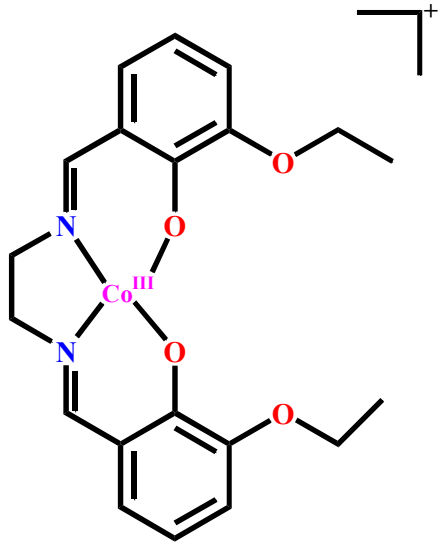

$[Co^{III}L^{2}]^{+}$, (**I**; $C_{20}H_{22}N_2O_4Co$)
m/z = 413, Intensity = 20%

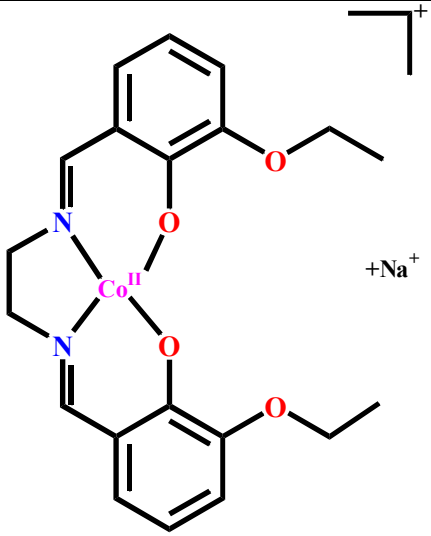

{$[Co^{II}L^{2}]+Na^{+}$}
(**II**; $C_{20}H_{22}N_2O_4CoNa$)
m/z =436, Intensity = 28%

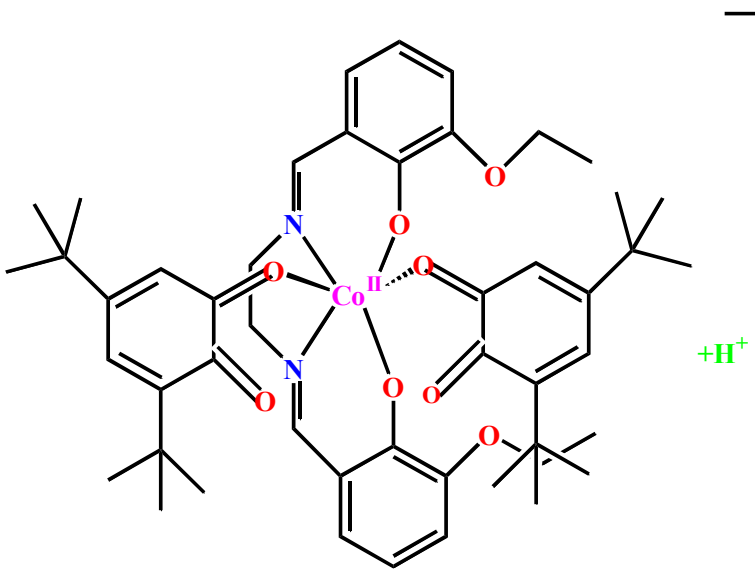

$[Co^{II}L^{2}(3,5\text{-DTBQ})_2+H^{+}]^{+}$ (**VIII**; $C_{48}H_{63}N_2O_8Co$)
m/z = 853, Intensity = 5%

5.4. Conclusions

To the best of our knowledge, The two cobalt(III) compounds $[Co^{III}L^{2}(N_3)_2\supset(H_3O^{+})]\cdot 2MeOH$ (**22**) and $[Co^{III}L^{2}(NCS)(H_2O)]\cdot DMF\cdot H_2O$ (**23**) are the first examples mononuclear cobalt(III) compounds from any type of ligands to show catecholase activity. The title Co^{III} compounds **22** and **23** are only the third examples of Co^{III} compounds derived from H_2L^{OEt} ligands and the first examples of Co^{III} compounds from these ligands where no decomposition of a part of the Schiff base ligand takes place.

Compound **22** is a unique example where a guest species (H_3O^{+} here) is trapped in $O(phenoxo)_2O(ethoxy)_2$ compartment of a system in which $N(imine)_2O(phenoxo)_2$ compartment of $[L^{OEt}]^{2-}$ is occupied by a trivalent metal ion. Coordination of a M^{III} ion by two anionic, apical ligands is also a new feature in 3-ethoxysalicylaldehyde─diamine ligand systems. It is also worth mentioning that, the special structural features in the Co^{III} compound, **22** have not been observed in any M^{III} (M = Fe, Mn, Co) compound derived from not only 3-ethoxysalicylaldehyde─diamine ligands but also from the closely similar 3-methoxysalicylaldehyde-diamine ligands.[1] All in all, structural diversity and crystal engineering aspects of 3-ethoxysalicylaldehyde-diamine ligands, which have been already observed as special ligands, have been further explored in this investigation.

References

(1) The Cambridge Structural Database (CSD), version 1.16, 2013. The Cambridge Crystallographic Data Center: Cambridge, U.K.

(2) O'Conner, C. J.; Freyberg, D. P.; Sinn, E. *Inorg. Chem.* **1979**, *18*, 1077.

(3) Bencini, A.; Benelli, C.; Caneschi, A.; Carlin, R. L.; Dei, A.; Gatteschi, D. *J. Am. Chem. Soc.* **1985**, *107*, 8128.

(4) Brewer, G. A.; Sinn, E. *Inorg. Chim. Acta* **1987**, *134*, 13.

(5) Gillon, B.; Cavata, C.; Schweiss, P.; Journaux, Y.; Kahn, O.; Schneider, D. *J. Am. Chem. Soc.* **1989**, *111*, 7124.

(6) Ruiz, R.; Lloret, F.; Julve, M.; Faus, J.; Muñoz, M. C.; Solans, X. *Inorg. Chim. Acta* **1993**, *213*, 261.

(7) Franceschi, F.; Solari, E.; Scopelliti, R.; Floriani, C. *Angew. Chem., Int. Ed.* **2000**, *39*, 1685.

(8) Karmakar, D.; Fleck, M.; Saha, R.; Layek, M.; Kumar, S.; Bandyopadhyay, D. *Polyhedron* **2013**, *49*, 93.

(9) Mandal, L.; Bhattacharya, S.; Mohanta, S. *Inorg. Chim. Acta* **2013**, *406*, 87.

(10) Chakraborty, P.; Mohanta, S. *Polyhedron* **2015**, *87*, 98.

(11) Mondal, S.; Mandal, S.; Carrella, L.; Jana, A.; Fleck, M.; Kohn, A.; Rentschler, E.; Mohanta, S. *Inorg. Chem.* **2015**, *54*, 117.

(12) Andruh, M.; Branzea, D. G.; Gheorghe, R.; Madalan, A. M. *CrystEngComm* **2009**, *11*, 2571.

(13) Costes, J.-P.; Dahan, F.; Dupuis, A.; Laurent, J.-P. *Inorg. Chem.* **1997**, *36*, 3429.

(14) Cunningham, D.; McArdle, P.; Mitchell, M.; Chonchubhair, N. N.; O'Gara, M.; Franceschi, F.; Floriani, C. *Inorg. Chem.* **2000**, *39*, 1639.

(15) Majumder, S.; Koner, R.; Lemoine, P.; Nayak, M.; Ghosh, M.; Hazra, S.; Lucas, C. R.; Mohanta, S. *Eur. J. Inorg. Chem.* **2009**, 3447.

(16) Bhattacharya, S.; Jana, A.; Mohanta, S. *CrystEngComm* **2013**, *15*, 10374.

(17) Bhattacharya, S.; Jana, A.; Mohanta, S. *Polyhedron* **2013**, *62*, 234.

(18) Biswas, A.; Mondal, S.; Mohanta, S. *J. Coord. Chem.* **2013**, *66*, 152.

(19) Jana, A.; Mohanta, S. *CrystEngComm* **2014**, *16*, 5494.

(20) Nayak, M.; Koner, R.; Lin, H.-H.; Flörke, U.; Wei, H.-H.; Mohanta, S. *Inorg. Chem.* **2006**, *45*, 10764.

(21) Hazra, S.; Koner, R.; Nayak, M., Sparkes, H. A.; Howard, J. A. K.; Dutta, S.; Mohanta, S. *Eur. J. Inorg. Chem.* **2009**, 4887.

(22) Sarkar, S.; Mohanta, S. *Rsc Adv.* **2011**, *1*, 640.

(23) Jana, A.; Majumder, S.; Carrella, L.; Nayak, M.; Weyhermueller, T.; Dutta, S.; Schollmeyer, D.; Rentschler, E.; Koner, R.; Mohanta, S. *Inorg. Chem.* **2010**, *49*, 9012.

(24) Chakraborty, P.; Majumder, S.; Jana, A.; Mohanta, S. *Inorg. Chim. Acta* **2014**, *410*, 65.

(25) Majumder, S.; Hazra, S.; Biswas, P.; Mohanta, S. *Polyhedron* **2009**, *28*, 2473.

(26) Majumder, S.; Dutta, S.; Carrella, L. M.; Rentschler, E.; Mohanta, S. *J. Mol. Struct.* **2011**, *1006*, 216.

(27) Hazra, S. Koner, R.; Nayak, M.; Sparkes, H. A.; Howard, J. A. K.; Mohanta, S.; *Cryst. Growth Des.* **2009**, *9*, 3603.

(28) Sasmal, S.; Majumder, S.; Hazra, S.; Sparkes, H. A.; Howard, J. A. K.; Nayak, M.; Mohanta, S. *CrystEngComm* **2010**, *12*, 4131.

(29) Nayak, M.; Jana, A.; Fleck, M.; Hazra, S.; Mohanta, S. *CrystEngComm* **2010**, *12*, 1416.

(30) Mondal, S.; Hazra, S.; Sarkar, S.; Sasmal, S.; Mohanta, S. *J. Mol. Struct.* **2011**, *1004*, 204.

(31) Jana, A.; Koner, R.; Nayak, M.; Lemoine, P.; Dutta, S.; Ghosh, M.; Mohanta, S. *Inorg. Chim. Acta* **2011**, *365*, 71.

(32) Jana, A.; Weyhermüller, T.; Mohanta, S. *CrystEngComm* **2013**, *15*, 4099.

(33) Ghosh, S.; Mandal, L.; Mohanta, S. *Polyhedron* **2015**, *97*, 1.

(34) Nayak, M.; Sarkar, S.; Lemoine, P.; Sasmal, S.; Koner, R.; Sparkes, H. A.; Howard, J. A. K.; Mohanta, S. *Eur. J. Inorg. Chem.* **2010**, 744.

(35) Sarkar, S.; Fleck, M.; Mohanta, S. *J. Mol. Struct.* **2012**, *1021*, 174.

(36) Desiraju, G. R. ed. *The Crystal as a Supramolecular Entity*, *Perspectives in Supramolecular Chemistry* 2, Wiley, London, 1996.

(37) Dutta, R.; Ghosh, P. *Chem. Commun.* **2014**, *50*, 10538.

(38) Agnihotri, P.; Suresh, E.; Paul, P.; Ghosh, P. K. *Eur. J. Inorg. Chem.* **2006**, 3369.

(39) Mishra, A.; Gupta, R. *Dalton Trans.* **2014**, *43*, 7668.

(40) Koval, I. A.; Gamez, P.; Belle, C.; Selmeczi, K.; Reedijk, J. *Chem*. *Soc*. *Rev*. **2006**, *35*, 814.

(41) Majumder, S.; Sarkar, S.; Sasmal, S.; Sañudo, E. C.; Mohanta, S. *Inorg*. *Chem*. **2011**, *50*, 7540.

(42) Kaizer, J.; Csonka, R.; Baráth, G.; Speier, G. *Trans*. *Met*. *Chem*. **2007**, *32*, 1047.

(43) Triller, M. U.; Pursche, D.; Hsieh, W.-Y.; Pecoraro, V. L.; Rompel, A. Krebs, B. *Inorg*. *Chem*. **2003**, *42*, 6274.

(44) Mukherjee, S. Weyhermüller, T.; Bothe, E.; Wieghardt, K.; Chaudhuri, P. *J*. *Chem*. *Soc*., *Dalton Trans*. **2004**, 3842.

(45) Jana, A.; Aliaga-Alcalde, N.; Ruiz, E.; Mohanta, S. *Inorg*. *Chem*. **2013**, *52*, 7732.

(46) Hitomi, Y.; Ando, A.; Matsui, H.; Ito, T.; Tanaka, T.; Ogo, S.; Funabiki, T. *Inorg*. *Chem*. **2005**, *44*, 3473.

(47) Simándi, T. L.; Simándi, L. I. *J*. *Chem*. *Soc*., *Dalton Trans*. **1999**, 4529.

(48) Lo, S.-I.; Lu, J.-W.; Chen, W.-J.; Wang, S.-R.; Wei, H.-H.; Katada, M. *Inorg*. *Chim*. *Acta* **2009**, *362*, 4699.

(49) Simándi, L. I.; Simándi, T. L. *J*. *Chem*. *Soc*., *Dalton Trans*. **1998**, 3275.

(50) Rao, C. R. K.; Zacharias, P. S. *Polyhedron* **1997**, *16*, 1201.

(51) Majumder, S.; Mondal, S.; Lemoine, P.; Mohanta, S. *Dalton Trans*. **2013**, *42*, 4561.

(52) Mandal, L.; Sasmal, S.; Sparkes, H. A.; Howard, J. A. K.; Mohanta, S. *Inorg*. *Chim*. *Acta* **2014**, *412*, 38.

(53) Mandal, L.; Mohanta, S. *Dalton Trans*. **2014**, *43*, 15737.

(54) Sheldrick, G. M. SAINT, Version 6.02, SADABS, Version 2.03; Bruker AXS, lnc.: Madison, WI, 2002.

(55) Sheldrick, G. M. SHELXTL, Version 6.10, Bruker AXS, lnc.: Madison, WI, 2002.

(56) Sheldrick, G. M. SHELXL-97, Crystal Structure Refinement Program; University of Göttingen: Göttingen, 1997.

(57) Thakurta, S. Butcher, R. J.; Pilet, G.; Mitra, S. *J*. *Mol*. *Struct*. **2009**, *929*, 112.

(58) Kia, R., Kargar, H.; Zare, K.; Khan, I. U. *Acta Crystallogr*. **2010**, *E66*, m366.

(59) Geary, W. J. *Coord*. *Chem*. *Rev*. **1971**, 7, 81.

(60) Abedin, T. S. M.; Thompson, L. K.; Miller, D. O. *Chem*. *Commun*. **2005**, 5512.

(61) Sutradhar, M.; Carrella, L. M.; Rentschler, E. *Polyhedron* **2012**, *38*, 297.

(62) Zhang, N.; Huang, C.-Y.; Shi, D.-H.; You, Z.-L. *Inorg. Chem. Commun.* **2011**, *14*, 1636.

(63) Hwang, I.-C.; Ha, K. *Z. Kristallogr.-New Cryst. Struct.* **2006**, *221*, 363.

(64) Vázquez-Fernández, M.Á.; Bermejo, M. R.; Fernández-García, M. I.; González-Riopedre, G.; Rodríguez-Doutón, M. J.; Maneiro, M. *J. Inorg. Biochem.* **2011**, *105*, 1538.

(65) Vázquez-Fernández, M. Á.; Fernández-García, M. I.; González-Riopedre, G.; Maneiro, M.; Rodríguez-Doutón, M. J.; *J. Coord. Chem.* **2011**, *64*, 3843.

(66) Ha, K. *Z. Kristallogr.-New Cryst. Struct.* **2010**, *225*, 257.

(67) Hwang, I.-C.; Ha, K. *Z. Kristallogr.-New Cryst. Struct.* **2006**, *221*, 365.

(68) Ma, X.-L.; You, Z.-L. *Trans. Met. Chem.* **2008**, *33*, 961.

(69) González-Riopedre, G.; Fernández-García, M. I.; González-Noya, A .M.; Vázquez-Fernández, M. Á.; Bermejo, M. R.; Maneiro, M. *Phys. Chem. Chem. Phys.* **2011**, *13*, 18069.

(70) Ha, K. *Z. Kristallogr.-New Cryst. Struct.* **2010**, *225*, 285.